Synthesis and sintering of nano-sized BaSnO₃ powders containing BaGeO₃

**Roberto Köferstein · Lothar Jäger ·
Mandy Zenkner · Francisco Javier García-García ·
Stefan G. Ebbinghaus**

Abstract The formation of solid solutions of the type $[Ba(HOC_2H_4OH)_4][Sn_{1-x}Ge_x(OC_2H_4O)_3]$ as $BaSn_{1-x}/Ge_xO_3$ precursor and the phase evolution during its thermal decomposition are described in this paper. The 1,2-ethanediolato complexes can be decomposed to nano-sized $BaSn_{1-x}/Ge_xO_3$ preceramic powders. Samples with $x = 0.05$ consist of only a $Ba(Sn,Ge)O_3$ phase, whereas powders with $x = 0.15$ and 0.25 show diffraction patterns of both the $Ba(Sn,Ge)O_3$ and $BaGeO_3$ phase. The sintering behaviour was investigated on powders with a $BaGeO_3$ content of 5 and 15 mol%. These powders show a specific surface area of 15.4–15.9 m^2/g and were obtained from calcination above 800 °C. The addition of $BaGeO_3$ reduced the sintering temperature of the ceramics drastically. $BaSn_{0.95}Ge_{0.05}O_3$ ceramics with a relative density of at least 90% can be obtained by sintering at 1150 °C for 1 h. The ceramic bodies reveal a fine microstructure with cubical-shaped grains between 0.25 and 0.6 μm. For dense ceramics, the sintering temperature could be reduced down to 1090 °C, when the soaking time was extended up to 10 h.

Introduction

Pure and doped barium stannate ($BaSnO_3$) as well as its solid solutions (e.g. $BaTi_{1-x}Sn_xO_3$) have found important applications in materials science and technology due to its dielectric properties, semiconducting behaviour and high thermal stability [1–3]. Because of these characteristic properties, $BaSnO_3$ based ceramics are becoming more and more important in materials technology. For example, $BaSnO_3$ can be used to prepare thermally stable capacitors and to fabricate ceramic boundary layer capacitors [4–12]. Furthermore, $BaSnO_3$ can be also used as a functional material for semiconductor gas sensors and photocatalytic applications [13–20]. $BaSnO_3$ crystallises in the perovskite-type structure and has a band gap of 3.4 eV [21]. Apart from the mixed-oxide method, which results in coarse-grained powders, some chemical syntheses have been developed to obtain fine-grained $BaSnO_3$ powders. Hydrothermal and sol–gel [22–25] synthesis as well as precursor complex, coprecipitation- and polymerized complex methods [26–29] are suitable to obtain fine-grained $BaSnO_3$ powders. Compacts on the basis of $BaSnO_3$ generally reveal only a moderate densification behaviour [5, 30–37]. Therefore, such ceramic bodies need high sintering temperatures or very long soaking times. In order to produce capacitor components based on $BaSnO_3$, dense (i.e. almost pore free) material bodies are required, because pores would act as a sink to the electrical charge carriers and would be the source of poor grain-to-grain connectivity and significant dielectric losses [34, 35, 38–42]. The densification behaviour can be improved and thus the sintering temperature can be reduced using fine-grained powders [30] or sintering aids [43, 44]. Kumar and Choudhary [45] sintered coarse-grained $BaSnO_3$ adding $BaSiO_3$, while Wang et al. [46] used SiO_2 as a sintering aid for $BaSnO_3$. Recently, we have investigated the effect of $BaGeO_3$ on the sintering properties and microstructures of both $BaSnO_3$ ceramic bodies prepared by the classical mixed-oxide method [47] and $BaTiO_3$-based ceramics [48].

R. Köferstein (✉) · L. Jäger · M. Zenkner · S. G. Ebbinghaus
Institut für Chemie, Anorganische Chemie, Martin-Luther-
Universität Halle-Wittenberg, Kurt-Mothes Strasse 2,
06120 Halle, Germany
e-mail: roberto.koeferstein@chemie.uni-halle.de

F. J. García-García
Lehrstuhl für Festkörperchemie, Institut für Physik, Universität
Augsburg, Universitätsstrasse 1, 86159 Augsburg, Germany

The present study deals with the preparation of a Ba(Sn,Ge)–1,2-ethanediolato complex precursor, including a sintering aid component, which can be decomposed to nano-sized $BaSn_{1-x}/Ge_xO_3$ powders. In this precursor, the components are evenly distributed on a molecular level, which leads to a more homogeneous distribution of the sintering aid in the resulting ceramic bodies. Additionally, phase evolution, the sintering behaviour of $BaSn_{1-x}/Ge_xO_3$ compacts as well as the microstructures of resulting ceramic bodies have been investigated.

Experimental

Material preparation

$[Ba(HOC_2H_4OH)_4][Sn_{1-x}Ge_x(OC_2H_4O)_3]$ precursor complexes were prepared analogously to the preparation of $[Ba(HOC_2H_4OH)_4][Sn(OC_2H_4O)_3]$ [30]. Ice-cold water (800 mL) was slowly added to fresh distilled $SnCl_4$ (0.10-x mol; p.a., *Laborchemie Apolda*) and then a concentrated ammonia solution was added to adjust a pH value of 7–7.5. The precipitate was slowly filtered-off and washed with water until the filtrate was almost free from Cl^- ions. A suspension of this wet precipitate ($SnO_2 \cdot nH_2O$) with $Ba(OH)_2 \cdot 8H_2O$ (0.10-x mol; puriss. p.a., *Fluka*) and 800 mL 1,2-ethanediol was stirred overnight at room temperature in an argon atmosphere. Thereafter, the suspension was heated at about 130 °C to remove water. Afterwards, $Ge(OC_2H_5)_4$ (x mol, *Alfa Aesar GmbH & Co KG*) and x mol $Ba(OH)_2 \cdot 8H_2O$ were added. The reaction mixture was heated at 120–130 °C for 8 h. About two thirds of the solvent was removed under reduced pressure at about 80 °C. The reaction mixture was then cooled to room temperature and diluted with propan-2-ol. The white, crystalline precipitate of $[Ba(HOC_2H_4OH)_4][Sn_{1-x}Ge_x(OC_2H_4O)_3]$ was filtered, washed with acetone, and dried at room temperature in vacuum.

For the shrinkage and sintering studies the precursor complexes with $x = 0.05$ and 0.15 were calcined in static air at 850 and 860 °C by a heating-rate controlled thermal treatment, as described below. The calcined powders were milled with ZrO_2-balls in propan-2-ol for 2 h (m_{powder}: $m_{balls} = 1:4$). After filtering and drying, the powders were mixed with 5 mass% of a saturated aqueous solution of polyvinyl alcohol (PVA) as a pressing aid, then the powders were pressed to discs with a green density of about 2.8–3.0 g/cm^3.

Characterization

X-ray powder diffraction (XRD) patterns were recorded on a *STOE* STADI MP diffractometer at 20 °C using $CoK\alpha_1$ radiation. Dilatometric (shrinkage) investigations were performed in a flowing synthetic air atmosphere (50 mL/min) in a TMA 92-16.18 unit from *Setaram*. The specific surface area was determined using nitrogen three-point BET (Nova 1000, *Quantachrome Corporation*). The equivalent BET particle diameter was calculated assuming the powder particles were spherical or cubic in shape [49]. Crystallite sizes were determined with the software suite WinXPOW [50] by XRD line broadening using the Scherrer equation [51] and the integral peak breadth. Scanning electron microscope images were recorded with a *Philips* XL30 ESEM (Environmental Scanning Electron Microscope) and transmission electron microscope images were recorded with a *Jeol* JEM 2100F.

Results and discussion

Solid solutions of the type $[Ba(HOC_2H_4OH)_4]$ $[Sn_{1-x}Ge_x(OC_2H_4O)_3]$

The non-isotypic 1,2-ethanediolato complexes $[Ba(HOC_2H_4OH)_4][Sn(OC_2H_4O)_3]$ (**1**) and $[Ba(HOC_2H_4OH)_2Ge(OC_2H_4O)_3]$ (**2**) can be used as precursors for fine-grained $BaSnO_3$ and $BaGeO_3$ powders [30, 52, 53]. We have prepared mixed precursor complexes of **1** and **2** up to a germanium content of 25 mol%. Since the XRD patterns of the Ba(Sn,Ge)–precursor complexes (Fig. 1b–d) show only the reflection pattern of complex **1** (Fig. 1a) it can be concluded that each precursor consists of a single phase indicating the formation of solid solutions of the type $[Ba(HOC_2H_4OH)_4][Sn_{1-x}Ge_x(OC_2H_4O)_3]$ up to $x = 0.25$. Furthermore, the insertion
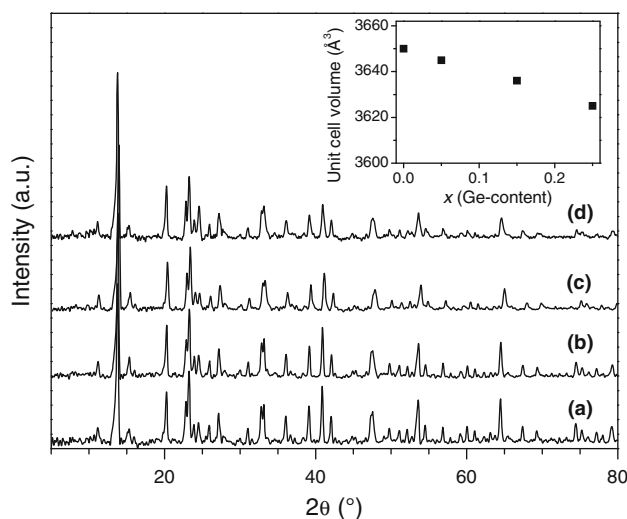
Fig. 1 XRD patterns of selected precursors. (*a*) $[Ba(HOC_2H_4OH)_4][Sn(OC_2H_4O)_3]$ (1), (*b–d*) $[Ba(HOC_2H_4OH)_4][Sn_{1-x}Ge_x(OC_2H_4O)_3]$, (*b*) $x = 0.05$ (**5**); (*c*) $x = 0.15$ (**15**); (*d*) $x = 0.25$ (**25**). The *inset* shows the relationship between the volume of the unit cell and the germanium content (*x*) of these complexes
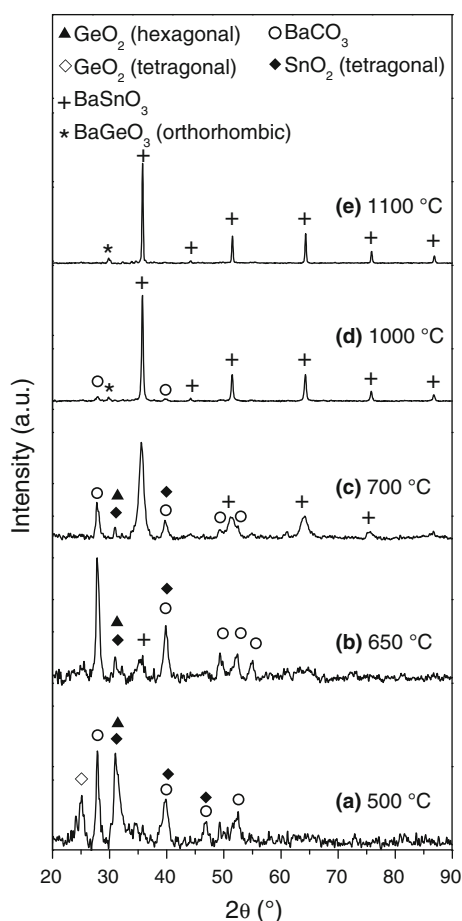
Fig. 2 XRD patterns of the $[Ba(HOC_2H_4OH)_4][Sn_{0.75}Ge_{0.25}(OC_2H_4O)_3]$ precursor (**25**) decomposed at various calcination temperatures (soaking time 1 h, heating rate 10 °C/min)

of Ge^{4+} into the crystal structure of **1** is connected to a decrease in unit cell volume (inset in Fig. 1).

Figure 2 represents XRD patterns of $[Ba(HOC_2H_4OH)_4]$ $[Sn_{0.75}Ge_{0.25}(OC_2H_4O)_3]$ (**25**, the number represents the germanium content) after different calcination steps in static air (heating rate 10 °C/min). Analogous to the calcination of the complexes **1** and **2**, precursor **25** disintegrated into $BaCO_3$, SnO_2 and GeO_2 at 500 °C. The XRD pattern (Fig. 2a) clearly shows reflections of orthorhombic $BaCO_3$ and tetragonal GeO_2 [54]. The reflection at $2\theta = 31.0°$ represents tetragonal SnO_2 and possibly hexagonal GeO_2 [54]. Heating at 650 °C (Fig. 2b) leads to a reduction of the intensities of reflections representing SnO_2 and GeO_2. The broad reflection around $2\theta = 35.5°$ indicates the evolution of $BaSnO_3$ [54]. Calcination at 700 °C for 1 h results in strong reflections of $BaSnO_3$, whereas the reflection for tetragonal GeO_2 disappears (Fig. 2c). XRD pattern after a heat treatment at 900 °C reveals the formation of orthorhombic $BaGeO_3$ (not shown) and at 1000 °C we clearly observe reflections of $BaSnO_3$ and orthorhombic $BaGeO_3$ (Fig. 2d). The small amount of $BaCO_3$ completely vanished

above 1000 °C (Fig. 2e). In ref. [47] it was observed a partial solid solubility of $BaGeO_3$ in $BaSnO_3$ of the order of 6–7 mol%. Therefore, the reflections of $BaSnO_3$ represent the perovskite phase $Ba(Sn,Ge)O_3$.

Shrinkage and sintering behaviour

Preceramic powders with $BaGeO_3$ contents of 5 mol% (**5**) and 15 mol% (**15**) were used for investigations of the sintering behaviour. Powders **5** and **15** were obtained after calcination of $[Ba(HOC_2H_4OH)_4][Sn_{0.95}Ge_{0.05}(OC_2H_4O)_3]$ and $[Ba(HOC_2H_4OH)_4][Sn_{0.85}Ge_{0.15}(OC_2H_4O)_3]$, respectively. The calcination procedure of **5** was as follows: heating at 10 °C/min to 500 °C, then slow heating at 1 °C/min to 850 °C, soaking for 3 h and cooling at 3 °C/min. Powder **15** was obtained in nearly the same manner, however, the precursor was heated up to 860 °C for 10 h. As seen in Fig. 7b, sample **5** consists of a $Ba(Sn,Ge)O_3$ perovskite phase and a small amount of $BaCO_3$. Whereas, powder **15** reveals reflections of a $Ba(Sn,Ge)O_3$ phase, small amounts of $BaCO_3$ and SnO_2 (Fig. 7a). The specific surface area (BET) of these powders was determined as 15.4 m^2/g (**5**) and 15.9 m^2/g (**15**), respectively. The equivalent particle size from these BET data was calculated as 55 nm, which can be considered as an average size of the primary particles [55]. Crystallite-size measurements by XRD line broadening [51] of the $Ba(Sn,Ge)O_3$ reflections reveal lower values of about $d_{crys.} = 22$ nm (**5**) and 24 nm (**15**), respectively. Discrepancies between the crystallite-/particle-size estimated by the XRD line broadening and the specific surface area were reported and explained elsewhere [43]. The decomposition of the precursor complexes leads to the development of an internal surface in the powder (closely joined crystallites), which is unavailable for nitrogen adsorption. Analogous discrepancies between the particle-/crystallite-size estimated by the XRD line broadening and the specific surface area were also observed in studies of ThO_2 and ZrO_2 [49, 56]. TEM images of powder **5** are seen in Fig. 3. The theoretical bulk densities of the resulting ceramic bodies were calculated as 7.12 g/cm^3 (**5**) and 6.85 g/cm^3 (**15**) [57].

The non-isothermal shrinkage behaviour (dilatometry) of powders **5** and **15** can be seen in Fig. 4. Both powders reveal the beginning of shrinkage at about 1000 °C, however, a significant shrinkage occurs above 1100 °C (**5**) and 1000 °C (**15**), respectively. Powder **15** begins to shrink at lower temperatures than powder **5**. On the other hand, powder **5** shows a very fast shrinkage process with a shrinkage rate maximum of −7.9%/min at 1240 °C. The intensity of the shrinkage process of sample **15** is lower. We observe one rate maximum at 1106 °C (−2.5%/min) and another broad one at 1242 °C (−1.5%/min). The small difference of the whole shrinkage of both samples is mainly caused by different green densities of the compacts.

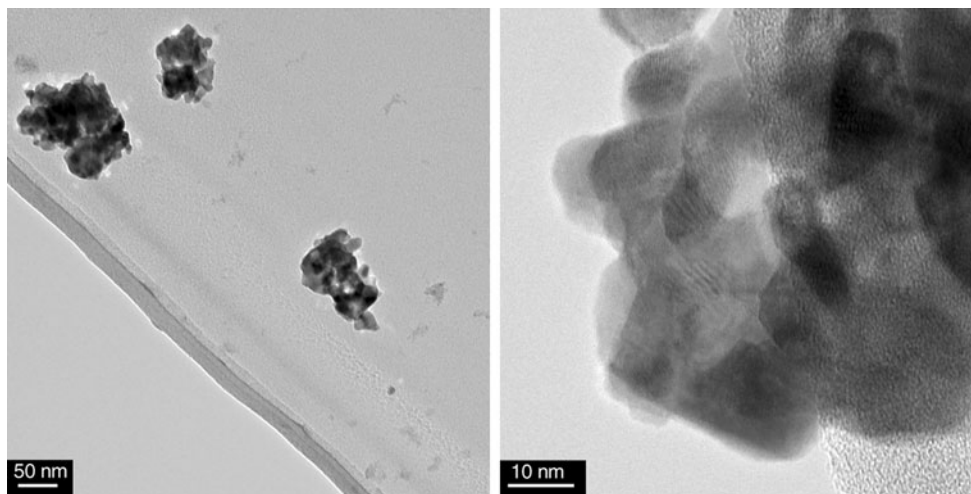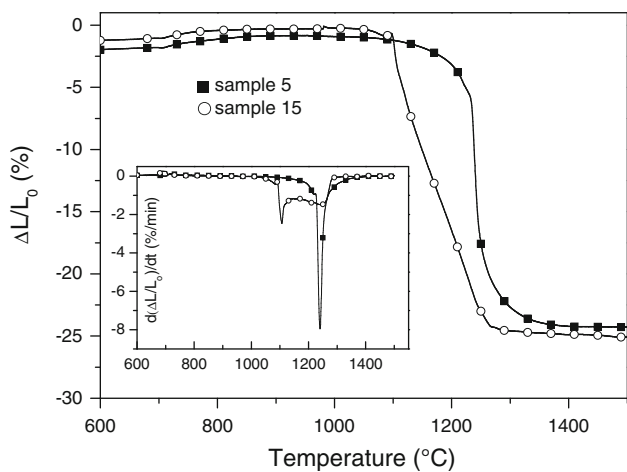**Fig. 3** TEM images of powder **5**

Fig. 4 Non-isothermal dilatometric measurements in air of green bodies of **5** and **15** (heating rate 10 °C/min). The *inset* shows the relative shrinkage rates of these samples

The final bulk densities of ceramic bodies (measured from their weight and dimensions) of **5** and **15** after conventional isothermal sintering for 1 and 10 h (heating rate 10 °C/min) are shown in Fig. 5. Dense ceramics (rel. density ≥ 90%) can be obtained after sintering at a minimum temperature of 1150 °C for 1 h (**5**), which is more than 400 K lower than for nano-BaSnO$_3$ without any additives [30] (Fig. 5a). The ceramic body reveals cubic grains in a small range between 0.25 and 0.6 μm (Fig. 6a). A higher BaGeO$_3$ content of 15 mol% (**15**) needs sintering temperatures considerable above 1150 °C to form dense ceramic bodies. The relative densities of samples **5** and **15** do not differ significantly above a sintering temperature of 1200 °C. Up to 1300 °C ceramic bodies with relative densities of 98–99% can be obtained (Fig. 5a). The final microstructures of ceramics of **5** after sintering of 1 h at 1200 °C show cubic or cuboid-like grains between about
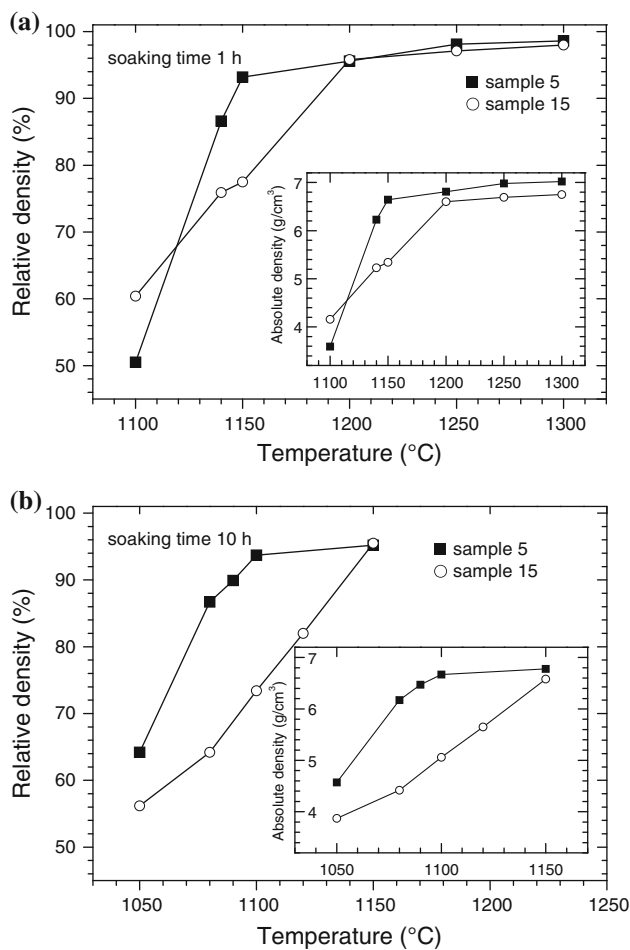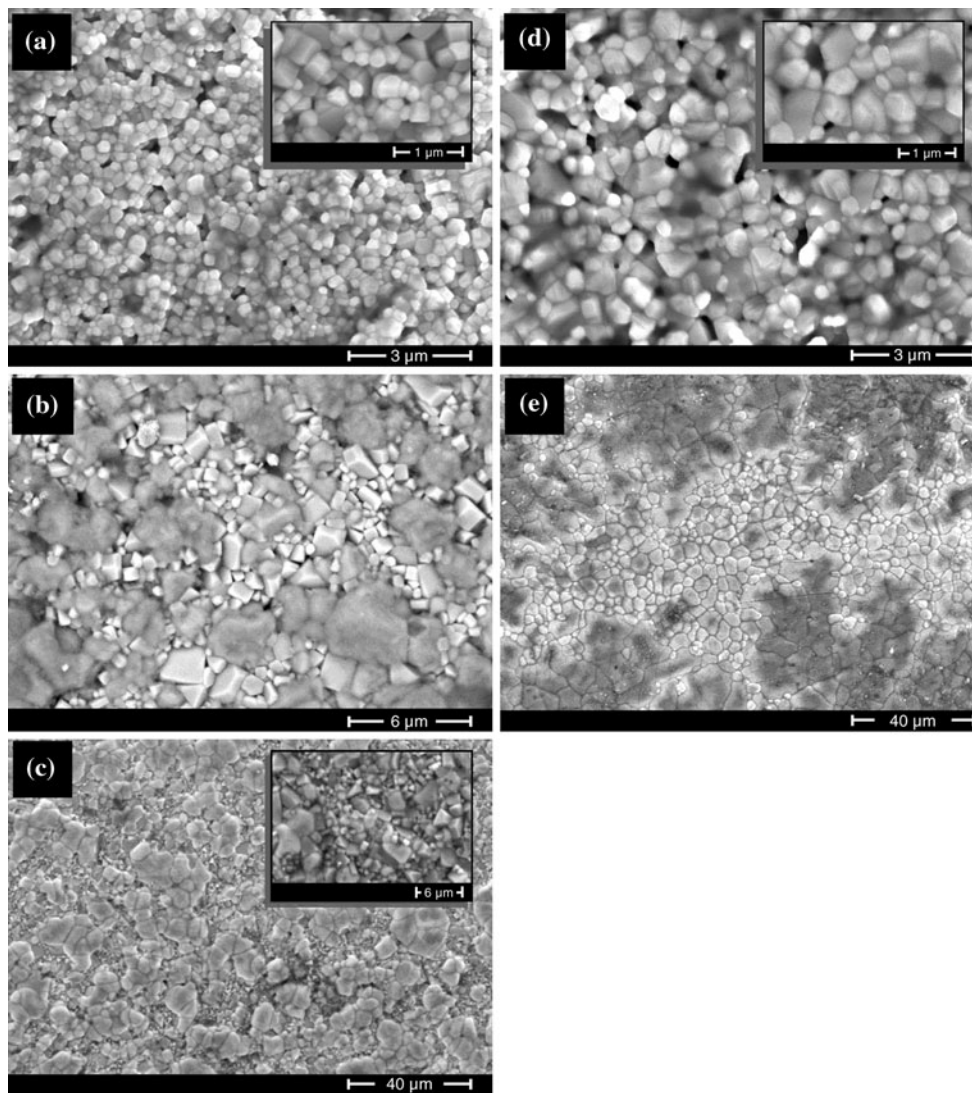

Fig. 5 Evolution of the final densities of some ceramic bodies of **5** and **15** after an isothermal sintering process of **a** 1 h and **b** 10 h (rate 10 °C/min)

0.25–2 μm, at 1250 °C a bi-modal grain-size distribution with grains between 0.5 and 5 μm (Fig. 6b), and at 1300 °C we found grains between 1.9 and 12 μm (Fig. 6c).

Fig. 6 SEM images of the surface of ceramic bodies of 5 after various sintering treatments (heating rate 10 °C/min). a 1150 °C, 1 h; b 1250 °C, 1 h; c 1300 °C, 1 h; d 1090 °C, 10 h; e 1150 °C, 10 h

The microstructures exhibit that small grains have a cubical- or cuboid-like shape, whereas larger grains have an increasingly irregular shape.

A prolonged soaking time of 10 h decreases the minimum sintering temperature for dense ceramic bodies down to 1090 °C (5) with grains in the range between 0.35 and 1 μm (Figs. 5b, 6d). A higher sintering temperature of 1150 °C (10 h) leads to a grain growth with irregular grains between 1.9 and 21 μm (Fig. 6e). Sample 15 requires temperatures above 1120 °C to reach relative densities of ≥90% (Fig. 5b). Compared to the microstructure of ceramics sintered for 1 h, we found more grains with an irregular shape after the prolonged sintering time. It can be seen that the absolute densities of ceramic bodies of 15 are almost always lower than of bodies of 5. As mentioned above, sample 15 has only a maximal

reachable density of 6.89 g/cm³, whereas sample 5 can achieve a maximum density of 7.12 g/cm³.

For comparison, $BaSnO_3$ compacts prepared by a precursor route without any additive show only very moderate sintering behaviour. Sintering temperatures above 1550 °C are necessary to reach a relative density of 90% [30].

Ceramic bodies of 5 exclusively show reflections of the $BaSnO_3$ phase; no other crystalline phase can be detected (Fig. 7c, d). Consequently, ceramic bodies of 5 consist of a solid solution between $BaSnO_3$ and $BaGeO_3$ ($BaSn_{0.95}Ge_{0.05}O_3$) [47]. By contrast, powder patterns of ceramics of 15 clearly indicate reflections of both the $Ba(Sn,Ge)O_3$ phase and the orthorhombic $BaGeO_3$ phase (Fig. 7e–g).

The isothermal sintering results clearly show that dense ceramic bodies can be obtained at sintering temperatures considerable below 1250 °C. As reported in ref. [47],
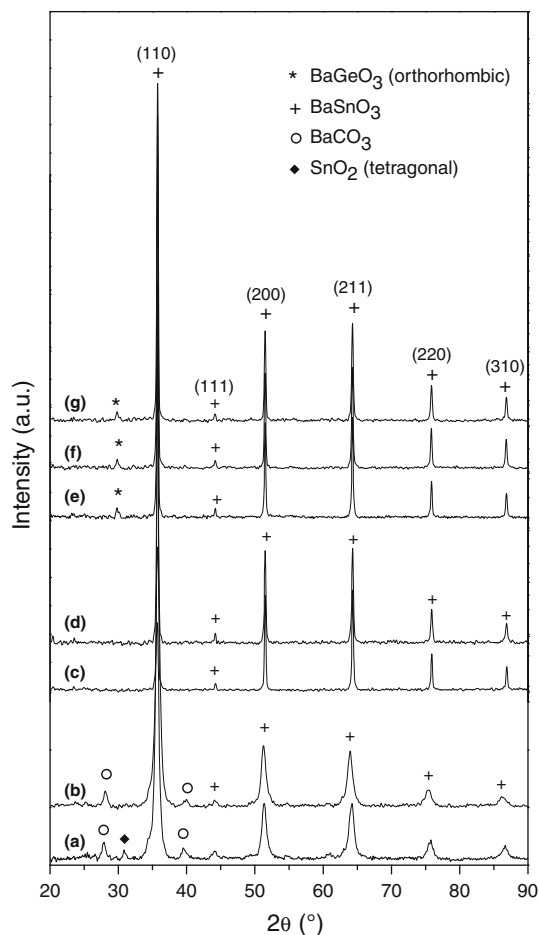
Fig. 7 Graphs (*a*) and (*b*) show the XRD patterns of the preceramic powders of precursor **15** (*a*) and **5** (*b*) resulting from a heating-rate controlled calcination process at 860 °C for 10 h (**15**) and 850 °C for 3 h (**5**), respectively. Graphs (*c–g*) represent XRD patterns of ceramic bodies after various sintering procedures. Ceramic **5**: (*c*) 1100 °C, 10 h; (*d*) 1300 °C, 1 h. Ceramic **15**: (*e*) 1150 °C, 10 h; (*f*) 1250 °C, 1 h; (*g*) 1300 °C, 1 h

$BaSnO_3$ and $BaGeO_3$ form a liquid phase at 1270 °C. As mentioned above, the non-isothermal dilatometric measurements (Fig. 4) show shrinkage maxima at temperatures <1270 °C and the maximum shrinkage rates ($\gg 0.1\%$/min) suggest that the shrinkage is dominated by sliding processes [58, 59]. That means, the formation of a liquid phase is not essential to form dense ceramic bodies and the densification process can be described as a solid-state sintering process. Consequently, the sintering additive $BaGeO_3$ does not act as a liquid phase former, primarily. $BaGeO_3$ as well as the small grain size of the preceramic powders (**5**, **15**) improve the sliding processes [60]. Such sliding processes are caused by defect-rich and amorphous (glass-like) contact boundaries, respectively [61–63]. Dror et al. [64] could show that these sliding processes (rearrangements) correlate also with the high amount of grain boundaries in nano-powders. They regarded the grain boundaries as amorphous areas surrounding crystalline cores, which promotes the sliding processes.

Conclusion

The sintering temperature of $BaSnO_3$ or $BaSnO_3$-based ceramics can be drastically lowered using both nano-sizes powders and sintering additive $BaGeO_3$. To combine both effects we synthesized $[Ba(HOC_2H_4OH)_4][Sn_{1-x}Ge_x(OC_2H_4O)_3]$ [$x = 0.05$ (**5**), 0.15 (**15**), 0.25 (**25**)] precursor complexes, which can be decomposed to nano-sized $BaSnO_3$ powders containing $BaGeO_3$. The decomposition of precursor **5** finally leads to a single-phase powder indicating a solid solution between $BaSnO_3$ and $BaGeO_3$. On the other hand, heat treatment of precursor **15** results in a powder and ceramic bodies containing both the $Ba(Sn,Ge)O_3$ perovskite phase and orthorhombic $BaGeO_3$. Isothermal sintering experiments of resulting compacts show a drastically reduced sintering temperature. Dense ceramic bodies of **5** can be obtained after sintering at 1150 °C for 1 h or at 1090 °C for 10 h, respectively. At these low sintering temperatures the ceramics have cubical-shaped grains between 0.25–0.6 µm and 0.35–1 µm, respectively.

References

1. Souza IA, Cavalcante LS, Sczancoski JC, Moura F, Paiva-Santos CO, Varela JA, Simões AZ, Longo E (2009) J Alloys Compd 477: 877
2. Shvartsman VV, Kleemann W, Dec J, Xu ZK, Lu SG (2006) J Appl Phys 99:124111
3. Müllert V, Beige H, Abicht H-P (2004) Appl Phys Lett 84:1341
4. Vivekanandan R, Kutty TRN (1990) Mater Sci Eng B 6:221
5. Singh P, Brandenburg BJ, Sebastian CP, Singh P, Singh S, Kumar D, Parkash O (2008) Jpn J Appl Phys 47:3540
6. Movchikova A, Malyshkina O, Suchaneck G, Gerlach G, Steinhausen R, Langhammer HT, Pientschke C, Beige H (2008) J Electroceramics 20:43
7. Wang T, Chen XM, Zheng XH (2003) J Electroceramics 11:173
8. Kumar A, Singh BP, Choudhary RNP, Thakur AK (2005) Mater Lett 59:1880
9. Prokopalo OI (1976) Ferroelectrics 14:683
10. Singh P, Kumar D, Parkash O (2005) J Appl Phys 97:074103
11. Brauer H (1970) Z Angew Phys 29:282
12. Wang X, Zhou F, Wang Z (2006) Dianzi Yuanjian Yu Cailiao 25:44
13. Ostrick B, Fleischer M, Hampe U, Meixner H (1997) Sens Actuators B 44:601
14. Tao S, Gao F, Liu X, Sørensen OT (2000) Sens Actuators B 71: 223
15. Chu X (2004) Mater Sci Eng B 106:305
16. Hodjati S, Vaezzadeh K, Petit C, Pitchon V, Kiennemann A (2000) Catal Today 59:323

17. Upadhyay S, Kavitha P (2007) Mater Lett 61:1912
18. Borse PH, Josh UA, Ji SM, Jang JS, Lee JS, Jeong ED, Kim HG (2007) Appl Phys Lett 90:0341031
19. Yuan Y, Lv V, Jiang X, Li Z, Yu T, Zou Z, Ye J (2007) Appl Phys Lett 91:0941071
20. Zhang Y, Zhang H, Wang Y, Zhang WF (2008) J Phys Chem C 112:8553
21. Larramona G, Gutierrez C, Pereira I, Nunes MR, da Costa FMA (1989) J Chem Soc Faraday Trans 85:907
22. Kutty TRN, Vivekanadan R (1987) Mater Res Bull 22:1457
23. Lu W, Schmidt H (2005) J Eur Ceram Soc 25:919
24. Cerda J, Arbiol J, Diaz R, Dezanneau G, Morante JR (2002) Mater Lett 56:131
25. Udawatte CP, Yoshimura M (2001) Mater Lett 47:7
26. Udawatte CP, Kakihana M, Yoshimura M (1998) Solid State Ion 108:23
27. Lu W, Schmidt H (2007) J Sol-Gel Sci Technol 42:55
28. Song YJ, Kim S (2001) J Ind Eng Chem 7:183
29. Jäger L, Lorenz V, Müller T, Abicht H-P, Rössel M, Görls H (2004) Z Anorg Allg Chem 630:189
30. Köferstein R, Jäger L, Zenkner M, Ebbinghaus SG (2009) J Eur Ceram Soc 29:2317
31. Singh P, Kumar D, Parkash O (2005) J Mater Sci Mater Electron 16:145
32. Upadhyay S, Parkash O, Kumar D (2001) J Mater Sci Mater Electron 12:165
33. Wie X, Yao X (2007) Mater Sci Eng B 137:184
34. Cernea M, Manea A, Piazza D, Galassi C, Vasile E (2007) J Am Ceram Soc 90:1728
35. Azad AM, Hon NC (1998) J Alloys Compd 270:95
36. Tien L-C, Chou C-C, Tsai D-S (2000) Ceram Int 26:57
37. Upadhyay S, Parkash O, Kumar D (2001) Mater Lett 49:251
38. Rice RW (1998) Porosity of ceramics. Marcel Dekker, New York, p 325
39. Marković S, Mitrić M, Cvjetićanin N, Uskoković D (2006) Mater Sci Forum 518:241
40. Singh P, Parkash O, Kumar D (2005) Solid State Ion 176:2167
41. He Z, Ma J, Zhang R (2004) Ceram Int 30:1353
42. Iddles DM, Bell AJ, Moulson AJ (1992) J Mater Sci 27:6303. doi:10.1007/BF00576276
43. Köferstein R, Jäger L, Zenkner M, Abicht H-P (2008) J Mater Sci 43:832. doi:10.1007/s10853-007-2195-4
44. Völtzke D, Abicht H-P (2000) Solid State Sci 2:149
45. Kumar A, Choudhary RNP (2007) J Mater Sci 42:2476. doi:10.1007/s10853-006-0804-2
46. Wang Z, Zhou F, Chen Z (2006) Dianzi Yuanjian Yu Cailiao 25:58
47. Köferstein R, Jäger L, Zenkner M, Müller T, Ebbinghaus SG (2010) J Eur Ceram 30:1419
48. Zenkner M, Jäger L, Köferstein R, Abicht H-P (2008) Solid State Sci 10:1556
49. Allred VD, Buxton SR, McBride JP (1957) J Phys Chem 61:117
50. Program WinXPOW v1.06 (1999) Stoe & Cie GmbH, Darmstadt
51. Neff H (1959) Grundlagen und Anwendung der Röntgen-Feinstruktur-Analyse. R. Oldenbourg, München, p 287
52. Köferstein R, Abicht H-P, Woltersdorf J, Pippel E (2006) Thermochim Acta 441:176
53. Köferstein R, Jäger L, Zenkner M, Abicht H-P (2007) Thermochim Acta 457:55
54. PDF 2 (International Centre for Diffraction Data, Pennsylvania) 2001, BaSnO$_3$ [15-780], BaCO$_3$ [5-378], SnO$_2$ [14-1445], GeO$_2$ [83-546$_{hexagonal}$; 73-1306$_{tetragonal}$], BaGeO$_3$ [37-137]
55. Buscaglia MT, Bassoli M, Buscaglia V, Alessio R (2005) J Am Ceram Soc 88:2374
56. Garvie RC (1965) J Phys Chem 69:1238
57. Marks GW, Monson LA (1955) Ind Eng Chem 47:1611
58. Schatt W (1992) Sintervorgänge. VDI-Verlag, Düsseldorf, p 78
59. Novikov II, Portnoj VK (1984) Superplastizität von Legierungen. Deutscher Verlag für Grundstoffindustrie, Leipzig, p.12 et seqq
60. Köferstein R, Jäger L, Zenkner M, Müller T, Abicht H-P (2008) Mater Chem Phys 112:531
61. Geguzin YaE, Klinchuk YuI (1976) Poroshkovaya Metallurgiya 7:17
62. Schatt W (1989) Z Metallkde 80:809
63. Schatt W (1992) Solid State Phenom 25–26:23
64. Dror Y, Levi RD, Baltianski S, Tsur Y (2006) J Electrochem Soc 153:F137